









Modeling and Analysis of Noise Reduction Method in SPAD-Based LiDAR System

Kai Ma , Tao Yin , *Member, IEEE*, Na Tian , *Member, IEEE*, Zhe Wang , Tian Zhao , Jian Liu ,
Nanjian Wu , *Member, IEEE*, and Liyuan Liu , *Member, IEEE*

Abstract—Ambient light interference stands as the primary source of noise encountered by the light detection and ranging (LiDAR) systems based on single-photon avalanche diode (SPAD), which seriously restricts the detection range and accuracy of sensors. Multi-event mode and time-gating method are extensively employed due to their effective suppression ability of the ambient light interference with easily implemented circuit structure. However, the current research on these two operational modes is limited to qualitative description, lacking a comprehensive theoretical analysis. This paper investigates the impact of the multi-event mode and time-gating method on enhancing the imaging capabilities of the sensor, employing a probability distribution perspective. A behavioral model is established, enabling the simulation of the comprehensive functionality of a SPAD-based LiDAR system in either first-hit mode or multi-event mode, including the histogramming, coincident detection, time-gating functions. The model can serve as a substitute for the actual circuit in system function validation and parameter optimization, thereby significantly reducing the design and simulation cycle.

Index Terms—Behavioral model, multi-event mode, SPAD, time of flight (ToF), time-gating mode.

I. INTRODUCTION

SINGLE-PHOTON avalanche diode (SPAD) image sensors are a prominent research focus in the industry due to their high sensitivity to single photons, straightforward imaging principle, and strong compatibility with CMOS technology. It finds primary applications in fields such as autonomous driving, 3D gaming, and fluorescent imaging [1], [2], [3], [4]. It employs the time-of-flight (ToF) principle by emitting pulsed laser light towards the target. The photons reflected by the target then travel back to the SPAD sensor along the same path. Once the sensor reacts, the time information is stored and subsequently processed by the Time-to-Digital Converter (TDC) to derive distance information, and presents the 3D features of the target. However, due to the single-photon sensitivity of SPAD, it cannot

effectively distinguish ambient photons from signal photons. Consequently, the presence of ambient light will cause great performance degradation for imaging. Therefore, suppressing ambient light is currently the main research direction of SPAD-based image sensor, while multi-event mode and time-gating method are commonly used technical methods.

The multi-event mode and first-hit mode are based on the response times of SPAD during a single laser emission. Compared to the latter, which only records the arrival time of the first photon in a single measurement, SPAD in multi-event mode can work continuously, ensuring the measurement ability for long-distance targets under high ambient light. As for the gating mode, it can divide the entire measurement window into several intervals and enable SPAD in segments. Due to the distribution of environmental photons throughout the entire time window, while signal photons are concentrated in a certain interval, time-gating mode can effectively improve the signal-to-background ratio (SBR) and thus enhance sensor detection capabilities.

In [5], the entire laser imaging detection and ranging (LiDAR) system is analyzed using a probabilistic model and simulation. A detailed comparison is conducted between the SBR and detection probability (DP) before and after coincident detection. In [6], a Monte-carlo simulator developed in Matlab for the analysis is present. Together with the modeling of the background noise and target topology, the fundamental factors inherent in a typical LiDAR acquisition system have been included in order to predict the achievable system. In [8] and [9], the operational principle of the coincident detection mode is theoretically analyzed, and a novel method based on the adaptive adjustment of photon coincidence detection is proposed, which can suppress the background light and simultaneously improve the dynamic range. The aforementioned investigations are all based on the first-hit mode of SPAD and have not utilized the model to study the working characteristics of multi-event mode.

In [10], the proposed behavioral simulation model provides a promising candidate tool for the developments of the SPAD based ToF sensors. But the modeling part is limited to the photon distribution and SPAD function, which does not involve the noise reduction technologies such as histogramming, coincident detection, multi-event mode, and time-gating. And the subsequent modules still use the actual circuit. This paper conducts a theoretical analysis of the multi-event mode and time-gating method, and constructs a comprehensive behavioral circuit model employing the Verilog-A hardware description language (HDL). A concise histogram circuit model has been

Manuscript received 23 September 2023; revised 31 October 2023; accepted 5 November 2023. Date of publication 9 November 2023; date of current version 22 November 2023. This work was supported in part by the National Natural Science Foundation of China under Grants 61974146 and 61874107, and in part by Beijing Municipal Science and Technology Project under Grant Z221100007722028. (*Corresponding authors: Tao Yin; Liyuan Liu.*)

The authors are with the State Key Laboratory of Superlattices and Microstructures, Institute of Semiconductors, Chinese Academy of Sciences, Beijing 100083, China, and also with the University of Chinese Academy of Sciences, Beijing 101408, China (e-mail: makai21@semi.ac.cn; yint@semi.ac.cn; liuly@semi.ac.cn).

Digital Object Identifier 10.1109/JPHOT.2023.3331384

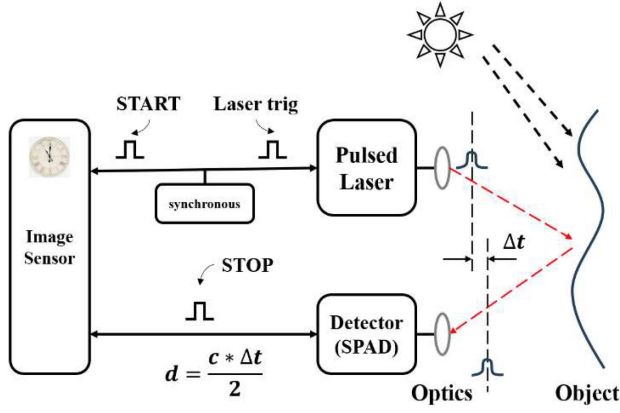


Fig. 1. Block diagram of a LiDAR system.

proposed, and the corresponding output results can be directly obtained based on peak information. Therefore, in addition to guiding the construction of histogram circuits, it can also be used to compare the effects of different working modes. By configuring relevant parameters, the functions of each module within the LiDAR system can be directly and quickly verified, providing a reliable basis for the subsequent circuit design.

II. PHOTON DISTRIBUTION

As shown in Fig. 1, a typical LiDAR system usually includes five parts [5], [6], [7]: the laser source, the optics, the target to be measured, the SPAD image sensor integrated with time-to-digital converters and the environment in which the target is placed.

The laser emitted by the laser source passes through the optics and forms the divergence angles of α_x and α_y in the horizontal and vertical directions respectively. If the target distance d is known, the area irradiated by it is A_{tx} . If the power of the laser source is P_{tx} , then the laser power per unit area is P_s .

$$A_{tx} = 4d^2 \tan\left(\frac{\alpha_x}{2}\right) \tan\left(\frac{\alpha_y}{2}\right) \quad (1)$$

$$P_s = \frac{P_{tx}}{A_{tx}} \quad (2)$$

The photons that reach the surface of the object are reflected and return to the image sensor. During the propagation process, the target reflectivity FT and lens efficiency TO will attenuate the optical power, and the attenuation coefficient $(\sin \alpha)^2$ will be considered at the same time.

$$(\sin \alpha)^2 = \frac{\left(\frac{D}{2}\right)^2}{\left(\frac{D}{2}\right)^2 + d^2} \approx \frac{D^2}{4d^2} \quad (3)$$

Considering that the focal length of the sensor lens is f and the aperture diameter is D , that is, the aperture coefficient $f_1 = f/D$, the detection area corresponding to a single pixel is A_{FOV} .

$$A_{FOV} = A_{pixel} \left(\frac{d}{f}\right)^2 \quad (4)$$

Assuming that the fill factor of the pixel is FF , the photon detection efficiency is PDE , and the energy of a single photon is hc/λ , so the number of signal photons received by a single pixel λ_s is

$$\begin{aligned} \lambda_s &= \frac{P_s \cdot A_{pixel} \cdot FT \cdot TO \cdot FF \cdot PDE \cdot \lambda}{4 \cdot f_1^2 \cdot h \cdot c} \\ &= \frac{P_{tx} \cdot A_{pixel} \cdot FT \cdot TO \cdot FF \cdot PDE \cdot \lambda}{4 \tan(\alpha_x/2) \tan(\alpha_y/2) \cdot 4 \cdot f_1^2 \cdot h \cdot c} \cdot \frac{1}{d^2} \quad (5) \end{aligned}$$

Most often, ambient light is the dominant source of noise, being several orders of magnitude (at least 2–3 orders of magnitude) higher than the detector dark count rate (DCR). Therefore, only ambient light will be considered for analysis in this paper. In addition, due to the lens placed at the front end of the sensor, the photons reflected from targets will become the main source of ambient light noise, while ambient photons directly entering the lens will occupy a small portion. Therefore, the number of ambient photons received λ_n is derived, by replacing P_s with the ambient light power P_n ,

$$\lambda_n = \frac{P_n \cdot A_{pixel} \cdot FT \cdot TO \cdot FF \cdot PDE \cdot \lambda}{4 \cdot f_1^2 \cdot h \cdot c} \quad (6)$$

The formulas (5) and (6) show that the number of signal photons received by a single pixel λ_s is inversely proportional to the square of the target distance d , while the number of ambient photons received λ_n is constant. So as the target distance increases, the influence of ambient photons is further intensified.

III. FIRST-HIT MODE AND MULTI-EVENTS MODE

When photons reach the SPAD sensor, according to the different working types of SPAD, it can be divided into first-hit mode and multi-event mode. In the first-hit mode, when a photon arrives, its output generates a pulse. And then if another photon arrives, it does not respond until the end of the period. The multi-event mode operates in an opposite way, the SPAD works continuously in the entire working period. The SPAD cannot respond to subsequent photons for a period of time after a photon responds, which is the so-called deadtime. For the first-hit mode, the circuit is easy to implement, and only one timestamp data is kept each pulse period, which can reduce the burden on the subsequent processing circuit. However, if the ambient light is strong and the target is far away, the correct result cannot be detected due to the pile-up effect [5]. While in the multi-event mode, SPAD can continue to record the next triggers in the event that the first photon is accidentally triggered by ambient photons. It can effectively suppress the pile-up effect, but will increase the amount of data accordingly.

The photon distribution of the most light sources and ambient photon are governed by Poisson statistics, and the time interval between adjacent photons obeys the exponential distribution. Therefore, the distribution probability of the photons can be predicted according to the characteristics of the above two distributions. For the first-hit mode, a theoretical analysis is carried out in [8]. When the first photon arriving at a certain moment, its distribution obeys the exponential distribution with $t = 0$ as the initial moment, and its probability density function

P_1 is

$$P_1 = \lambda e^{-\lambda t} \quad (7)$$

Unlike ambient photons that are distributed throughout the detection window, signal photons only exist during the pulse period of the laser emission. Therefore, when considering the influence of the signal photons, it is necessary to consider the overall distribution in sections. For the case of first-hit mode, there are only ambient photons considered before the arrival of signal photons, which means

$$P_1(t < t_0) = \lambda_n e^{-\lambda_n t} \quad (8)$$

where λ_n is the ambient photon rate. Therefore, the probability of false triggering of SPAD, that is, the probability of detecting ambient photons before t_0 is

$$P_1(t < t_0)_{int} = \int_0^{t_0} \lambda_n e^{-\lambda_n t} dt = 1 - e^{-\lambda_n t_0} \quad (9)$$

where t_0 is the moment when the signal photons start to be received. According to the result of formula (9), the probability of not detecting photons before t_0 is $1 - (1 - e^{-\lambda_n t_0}) = e^{-\lambda_n t_0}$. At t_0 , the incident photons include two parts, ambient photons and signal photons. If the influence of previous detection results is not considered, the probability of detecting ambient photons is λ_n and the probability of detecting signal photons is λ_s . However, considering the impact of previous detection results, using the conditional probability formula, the probability of detecting photons at t_0 is

$$\begin{aligned} P_1(t = t_0) &= \lambda_s e^{-\lambda_n t_0} + \lambda_n e^{-\lambda_n t_0} \\ &= (\lambda_s + \lambda_n) e^{-\lambda_n t_0} \end{aligned} \quad (10)$$

where λ_s is the photon rate of the signal light. In the period $t_0 \sim t_1$, (t_1 is the moment when signal photons stop to be received) the ambient photons and signal photons exist at the same time, so the distribution of photons obey the exponential with the parameter $(\lambda_s + \lambda_n)$. The corresponding probability density function is

$$P_1(t_0 < t < t_1) = e^{\lambda_s t_0} (\lambda_s + \lambda_n) e^{-(\lambda_n + \lambda_s)t} \quad (11)$$

The coefficient $e^{\lambda_s t_0}$ can be derived according to the value of P_1 at t_0 . The probability of right triggering of SPAD, that is, the probability of detecting photons during t_0 to t_1 is

$$\begin{aligned} P_1(t_0 < t < t_1)_{int} &= \int_{t_0}^{t_1} e^{\lambda_s t_0} \cdot (\lambda_s + \lambda_n) \cdot e^{-(\lambda_n + \lambda_s)t} dt \\ &= e^{-\lambda_n t_0} \cdot \left(1 - e^{-(\lambda_n + \lambda_s)(t_1 - t_0)}\right) \end{aligned} \quad (12)$$

Similar to the method for solving $P_1(t = t_0)$, At t_1 , only ambient photons exist. Considering the probability that no photons were detected before t_1 , using the conditional probability formula, we can obtain the probability density function of photons at t_1 is

$$\begin{aligned} P_1(t = t_1) &= (1 - P_1(t < t_1)_{int}) \cdot \lambda_n \\ &= e^{-\lambda_n t_0} \cdot e^{-(\lambda_n + \lambda_s)(t_1 - t_0)} \cdot \lambda_n \\ &= e^{-(\lambda_n + \lambda_s)(t_1 - t_0)} \cdot \lambda_n \cdot e^{-\lambda_n t_0} \end{aligned} \quad (13)$$

TABLE I
SYSTEM AND SIMULATION PARAMETERS USED IN THE BEHAVIORAL MODEL

Parameter	Operating condition	Deg. rate	Deg. cost
α_{low}	High power	20.34 $\mu\text{V/h}$	1.57 \$/h
α_{high}	Low power	23.48 $\mu\text{V/h}$	1.81 \$/h
β	Transient loading	0.0441 $\mu\text{V/kw}$	0.0034 \$/kW
W_l	Laser width	5ns	
P_n	ambient light intensity	15Klux	
f_1	aperture coefficient	1/1.4	
α_x	Laser divergence angle	60°	
α_y	(H/V)	0.25°	
FT	Target reflectance	20%	
TO	Optics efficiency	50%	
A_{pixel}	Pixel area	400 μm^2	
λ	Laser wavelength	905nm	
FF	Fill factor	30%	
PDE	Photon detection efficiency	8%	

The probability density function of photons after t_1 is

$$P_1(t > t_1) = e^{-\lambda_s(t_1 - t_0)} \cdot \lambda_n \cdot e^{-\lambda_n t} \quad (14)$$

And the probability of false triggering of SPAD, that is, the probability of detecting ambient photons after t_1 is

$$\begin{aligned} P_1(t > t_1)_{int} &= \int_{t_1}^{\infty} e^{-\lambda_s(t_1 - t_0)} \cdot \lambda_n \cdot e^{-\lambda_n t} dt \\ &= e^{-\lambda_s(t_1 - t_0)} \cdot e^{-\lambda_n t_1} \end{aligned} \quad (15)$$

Obviously,

$$P_1(t < t_0)_{int} + P_1(t_0 < t < t_1)_{int} + P_1(t > t_1)_{int} = 1 \quad (16)$$

To present the characteristics of the LiDAR system in a more intuitive manner, we utilize an actual scenario as an illustrative example. These parameters come from a sensor we are currently designing. A 905 nm laser wavelength with peak power of 400 W was used for analysis purposes simply because of the practical availability of such a laser in view of future measurements using that laser. A f-number of 1.4 was assumed to collect light onto a 128 × 128 SPAD sensor. The key model parameters are listed in Table I.

According to (5) and (6), By substituting the above parameters, the ambient photon rate $\lambda_n = 23.5 \times 10^6$ counts /sec, the signal photon rate $\lambda_s = 85/d^2 \times 10^9$ counts /sec. Assuming the target distance d is 15 m, then the photon distribution probability density function curve corresponding to this distribution is shown in Fig. 2.

According to (9) and (12), for the conditions corresponding to the above parameters, the probability of detecting ambient photons before t_0 is $P_1(t < t_0)_{int} = 1 - e^{-2.35} = 0.9$, far greater than the signal light detection probability during t_0 to t_1 , which is $P_1(t_0 < t < t_1)_{int} = e^{-2.35} \cdot (1 - e^{-(23.5 \times 10^6 + 85/225 \times 10^9) \times 5 \times 10^{-9}}) = 0.083$, even if the signal power is high (the SBR is about 12.6 dB if d is 15 m). So when detecting long-distance targets under strong background light, even if the signal power is high enough, the probability of getting

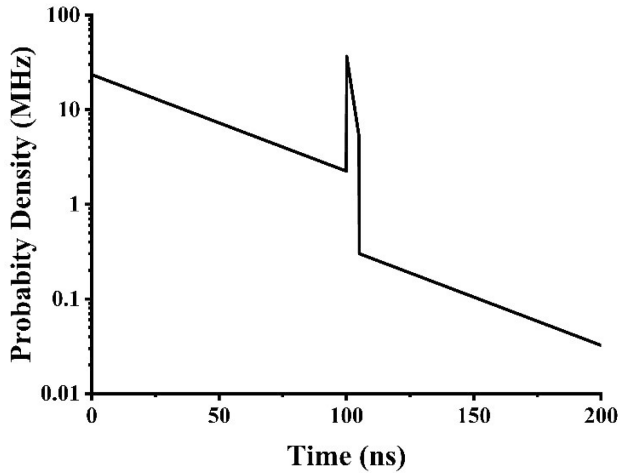


Fig. 2. Photon distribution of the first-hit mode.

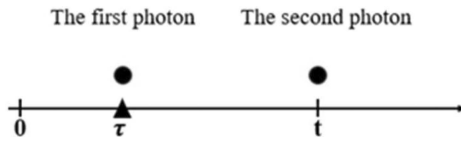


Fig. 3. The distribution of the second photon.

the correct result will be extremely low due to the serious pile-up effect. For the case corresponding to Fig. 2, in order to achieve a measurement distance of 15 m, it is necessary to try to reduce the number of ambient photons received while ensuring the SBR remains unchanged. According to the conclusion of formulas (5) and (6), one possible approach is to place filters to reduce the parameter TO. As a comparison, by reducing TO to 25%, the probability of detecting ambient photons before t_0 is $P_1(t < t_0)_{int} = 1 - e^{-2.35/2} = 0.69$ and the signal photons detection probability during t_0 to t_1 , which is $P_1(t_0 < t < t_1)_{int} = e^{-2.35/2} * (1 - e^{-(23.5 \times 10^6 + 85/225 \times 10^9) \times 5 \times 10^{-9}/2}) = 0.196$. Obviously, this method not only reduces the detection probability of ambient photons, but also greatly improves the detection probability of signal photons, providing important reference for determining relevant parameters.

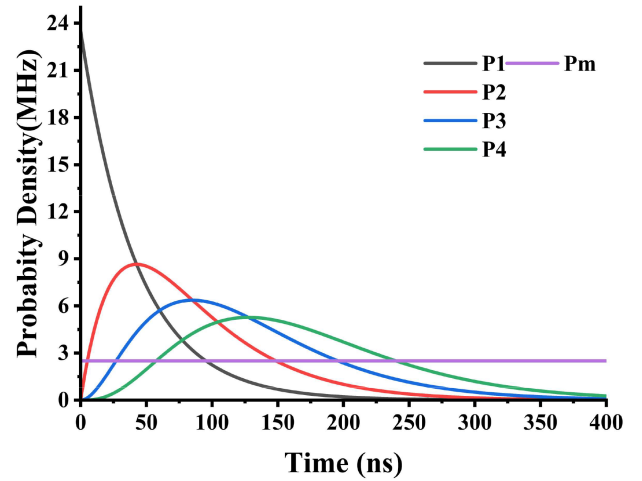
For the multi-event mode, since the SPAD works continuously, it is necessary to consider the distribution of other photons besides the first photon. As shown in Fig. 3, Considering the case when two photons are detected within the period $0 \sim t$.

If the second photon is detected at time t , then the first photon may be detected at any time between 0 and t . Traversing all the situations, we can get the distribution of the second photon P_2

$$P_2 = \int_0^t \lambda e^{-\lambda\tau} \cdot \lambda e^{-\lambda(t-\tau)} d\tau = \lambda^2 t \cdot e^{-\lambda t} \quad (17)$$

Using the similar method, the distribution of the k_{th} photon can be obtained. According to the distribution of the $(k-1)$ photons, the distribution of the k_{th} photon is

$$P_k = \int_0^t P_{k-1}(\tau) P_1(t-\tau) d\tau = \frac{\lambda^k \cdot t^{k-1}}{(k-1)!} e^{-\lambda t} \quad (18)$$

Fig. 4. Probability of detecting the k_{th} photon in multi-event mode.

The distribution P_k obeys the Erlang distribution. For the multi-event mode, the probability of detecting a photon at a certain time t is P_m , which is the sum of the distribution probabilities of all individual photons, after normalization

$$P_m = P_1 + P_2 + \dots + P_k = \text{norm} \left(\sum_{i=1}^k P_i \right) \quad (19)$$

Assuming that the photon rate $\lambda = 23.5 \times 10^6$ counts /sec, the window width is 400 ns, then the probability of detecting photons in the multi-event mode is shown in Fig. 4.

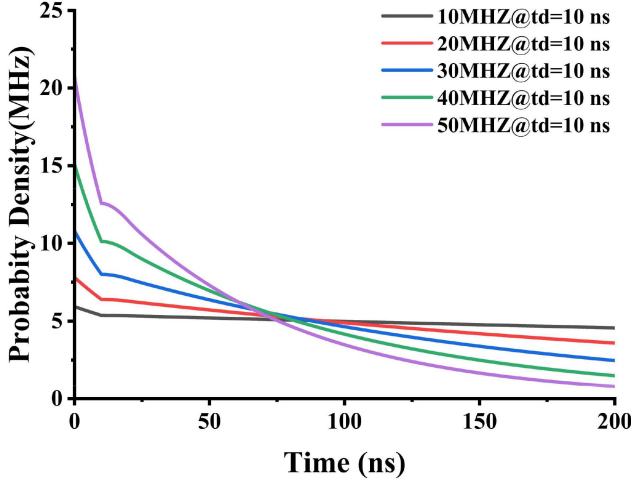
Obviously, for the multi-event mode, when the value of k is large enough, the probability of detecting photons P_m at each time point is equal. But this is only the distribution of photons arriving to the SPAD, not the response of the SPAD. The influence of the dead time of the SPAD is not considered.

Because the quenching and recovery process of SPAD takes a certain amount of time, during this period, even if photons arrive, SPAD does not respond, that is, the dead time td . For the SPAD working in the first-hit mode, since only the distribution of the first photon is considered, the influence of the dead time does not need to be considered, but for multi-event mode, since the SPAD continuously detects, the existence of the dead time will affect the output of the SPAD. For a SPAD operating in multi-event mode, its response to the first photon is consistent with the first-hit mode, which is not affected by dead time, so the detection probability of the first photon after considering the influence of dead time is $P_{1,d}$

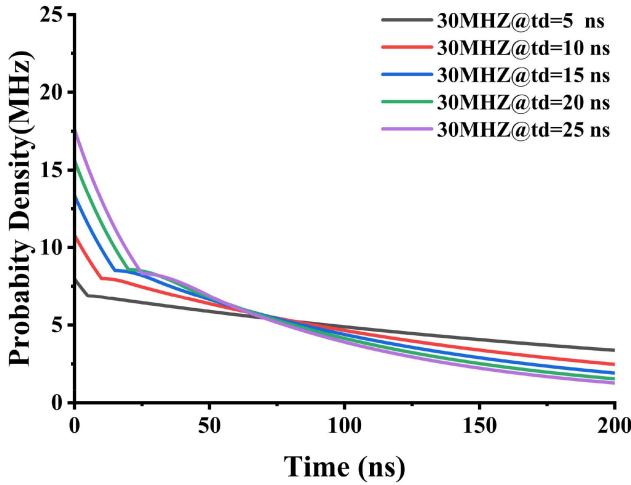
$$P_{1,d} = P_1 = \lambda e^{-\lambda t} \quad (20)$$

Similar to the situation in Fig. 3, considering the case when two photons are detected within the period $0 \sim t$, the detection probability of the second photon after considering the influence of dead time is $P_{2,d}$ if $\tau < t - td$,

$$P_{2,d} = P_2 = \int_0^t \lambda e^{-\lambda\tau} \cdot \lambda e^{-\lambda(t-\tau)} d\tau \quad (21)$$



(a)



(b)

Fig. 5. Photon distribution probability density function of multievents mode (a) with different photon rate λ (b) with different dead time td .

If $\tau > t - td$, due to the deadtime of SPAD,

$$P_{2,d} = 0 \quad (22)$$

So

$$P_{2,d} = \int_0^{t-t_d} \lambda e^{-\lambda\tau} \cdot \lambda e^{-\lambda(t-\tau)} d\tau = \lambda^2 (t - t_d) e^{-\lambda t} \quad (23)$$

Using the similar method, the distribution of k_{th} photon can be obtained. The photon detection probability of the k_{th} photon after considering the influence of dead time is

$$\begin{aligned} P_{k,d} &= \int_0^{t-t_d} P_{k-1,d}(\tau) P_{1,d}(t) d\tau \\ &= \frac{\lambda^k (t - (k-1)t_d)^{k-1}}{(k-1)!} e^{-\lambda t} \end{aligned} \quad (24)$$

It can be obtained by iteration, for the case of $(k-1)td < t < ktd$, the probability of detecting a photon after considering the influence of dead time is $P_{m,d}$

$$P_{m,d} = \text{norm} \left(\sum_1^k P_{k,d} \right) \quad (25)$$

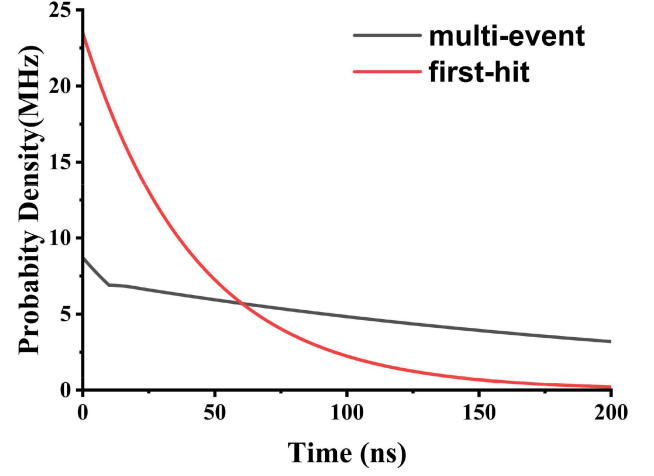


Fig. 6. Photon distribution probability density function of multievents mode vs first-hit mode.

Assuming the photon rate $\lambda = 10 \sim 50 \times 10^6$ counts/sec, the window width is 200 ns, and the dead time td is 5~25 ns. The photon distribution probability of multi-event mode is shown in Fig. 5.

According to Fig. 5(a), the corresponding probability of multi-event mode no longer remains constant, but gradually decreases with time. At the same time, the larger the λ , the faster the probability distribution decreases, which means that when the λ is larger, the dead time has a more obvious impact on the SPAD response. In addition, when the signal photon arrives at t_0 , it needs to consider the interference of the ambient light during $(t_0 - t_d) \sim t_0$, it means that in the scenario corresponding to Fig. 5(a), reducing the number of ambient photons before 75 ns can effectively improve the detection probability of signal light, while after 75 ns, this effect is not obvious, and even reduces the detection probability of signal photons. Similarly, according to Fig. 5(b), it can be concluded that reducing the dead time before 75 ns can effectively improve the probability of signal photons detection, while after 75 ns, this effect is not obvious, and even reduces the detection probability of signal photons. For the improvement of dead time, it can be achieved by improving the quenching and recovery circuit of SPAD, adding an active quenching branch, which can accelerate quenching and recovery, and thereby reduce dead time.

Therefore, in order to achieve a larger imaging range, it is not enough to simply increase the optical power. It is also necessary to minimize the deadtime of the SPAD.

A comparison between the distribution probability of the first-hit mode and that of the multi-event mode with $\lambda = 23.5 \times 10^6$ counts/sec and td is 10 ns is shown in Fig. 6.

From Fig. 6, it can be concluded that when the signal photon arrives at t_0 , it only needs to consider the interference of the ambient light during $(t_0 - t_d) \sim t_0$, instead of the period during $0 \sim t_0$, which can greatly improve the detection probability of the signal photon. Taking $t = 100$ ns, i.e., 15 m, as an example, compared with the first-hit mode, the probability can be increased more than 4 times.

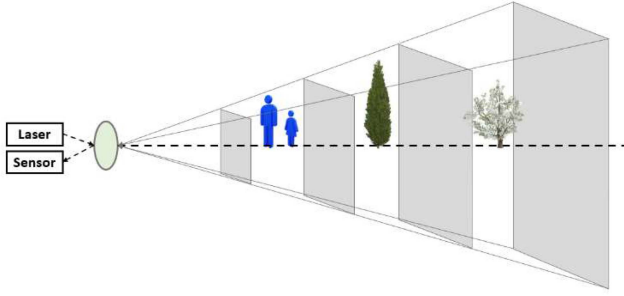


Fig. 7. Diagram of Time-Gating principle.

IV. TIME-GATING

As shown in Fig. 7, Time-Gating [11] refers to that if the target distance is unknown during actual detection, the entire time window can be divided into N intervals. And the sensor is turned on in turn, which can effectively reduce the interference of ambient light and increase SBR by N times [12], [13]. However, this approach will lead to an increase in data volume, subsequently resulting in a reduction of the sensor's frame rate.

In the first-hit mode, if the entire interval is divided into N parts, when a certain interval is detected separately, it can be divided into two situations for analysis. Considering the simplest case, the entire detection window is t_w , dividing the entire photon into two parts, and the time when the photon arrives as t_0 , and $t_0 > \frac{t_w}{2}$.

One intuitive way is the SPAD-Gating. The SPAD is turned on in the certain interval $\frac{t_w}{2} \sim t_w$, the opening time t_w can be equivalent to the initial time, so the photon detection probability P_{SG} is

$$P_{SG} = \begin{cases} 0 & t < \frac{t_w}{2} \\ \lambda e^{-\lambda(t - \frac{t_w}{2})} & \frac{t_w}{2} < t < t_0 \end{cases} \quad (26)$$

According to (12), during t_0 to $t_0 + Laserwidth$

$$P_{SG,int} = e^{-\lambda_n(t_0 - \frac{t_w}{2})} \cdot (1 - e^{-(\lambda_n + \lambda_s)laserwidth}) \quad (27)$$

According to (12) and (27), the ratio of signal photons detection probability after and before gating is

$$\frac{P_{SG,int}}{P_{S,int}} = \frac{e^{-\lambda_n(t_0 - \frac{t_w}{2})} \cdot (1 - e^{-(\lambda_n + \lambda_s)laserwidth})}{e^{-\lambda_n t_0} \cdot (1 - e^{-(\lambda_n + \lambda_s)laserwidth})} = e^{\lambda_n \frac{t_w}{2}} \quad (28)$$

Obviously, the using of gating can effectively suppress the pile-up effect, and a excellent effect can be obtained by setting the gating interval reasonably. Another method is the TDC-Gating. This method is especially suitable for sensors that adopt the column sharing TDC mode, because a column of pixels corresponds to only one TDC, and only one control line is required. Turning on TDC in the corresponding interval, the photon detection probability P_{TG} is

$$P_{TG} = \begin{cases} 0 & t < \frac{t_w}{2} \\ \lambda e^{-\lambda t} & \frac{t_w}{2} < t < t_0 \end{cases} \quad (29)$$

According to (12), during TOF to $TOF + Laserwidth$,

$$P_{TG,int} = e^{-\lambda_n t_0} \cdot (1 - e^{-(\lambda_n + \lambda_s)laserwidth}) \quad (30)$$

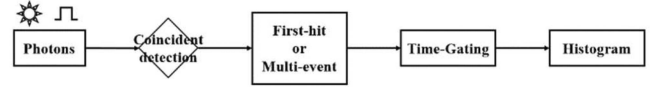


Fig. 8. Behavior model of LiDAR system.

After normalization,

$$\begin{aligned} P_{TG,int,nor} &= \frac{e^{-\lambda_n t_0} \cdot (1 - e^{-(\lambda_n + \lambda_s)laserwidth})}{1 - \int_0^{\frac{t_w}{2}} \lambda_n e^{-\lambda_n t} dt} \\ &= e^{-\lambda_n(t_0 - \frac{t_w}{2})} \cdot (1 - e^{-(\lambda_n + \lambda_s)laserwidth}) \\ &= P_{SG,int} \end{aligned} \quad (31)$$

This means that although the TDC-Gating mode does not directly improve the detection probability of signal photons, it can indirectly improve the detection probability of signal photons by suppressing the ambient light interference in the $0 \sim t_0$ period (in this period, even if the SPAD responds, TDC does not quantify), and this way can achieve the same effect as SPAD-Gating. Considering that the control of SPADs is usually difficult to achieve directly, which takes a considerable period of time, and requires a large number of control signals for a large-scale SPAD array, resulting in difficulties in layout and routing, TDC-Gating is a more effective circuit way.

V. BEHAVIORAL MODELING

In order to more intuitively verify the above-mentioned theoretical model and the functionality of other noise reduction circuits, it is necessary to conduct behavioral modeling of the entire SPAD-based LiDAR system. On the one hand, the constructed system model can be used to generate the photon distribution required for simulation, and then the response signal of SPAD can be obtained as the input signal of the subsequent processing circuit. On the other hand, processing circuits can be built using the ideal circuits generated by VerilogA, and gradually replaced with actual circuits, which is beneficial for debugging the functions of each module. Simultaneously, employing Verilog-A to articulate the circuit's functions and create a behavioral model facilitates a comprehensive understanding of the circuit, aids in parameter determination, and expedites the process of simulation verification.

In [10], the model in Fig. 1 is used for the light source and the TOF imaging pixel unit circuit simulation, but the subsequent processing circuit uses the actual circuit, such as TDC and Histogram circuit. In this paper, to achieve quick and precise validation of various design approaches, all processing circuits are directly substituted with Verilog-A models, as depicted in Fig. 8. For both the first-hit mode and the multi-event mode, corresponding circuit models can be established for selection according to different working scenarios. Among them, the multi-event mode needs to consider the impact of the SPAD dead time, and its value is generally 5 ns~15 ns.

After the output of the SPAD is received, the moment when the photon arrives is recorded, so as to obtain the distance

Algorithm 1: Verilog-A HDL Pseudocodes for Histogram Module.

```

module HIS(IN1,BIN,OUT);
  input SIGNAL; //The response of SPAD
  input BIN; //Periodic square wave signal
  output OUT;
  voltage SIGNAL, BIN, OUT;
  real OUT1, NUM; //The number of photons
  /*****define function*****/
  analog begin
    @(initial_step) begin
      NUM = 0;
      OUT1 = 0;
    end
    @(cross(V(SIGNAL) - TH, -1))
      NUM = NUM + 1;
    @(cross(V(BIN) - TH, +1))
      OUT1 = NUM;
    @(cross(V(BIN) - TH, +1))
      NUM = 0;
    V(OUT) <+ transition(OUT1, td, tt);
  end
endmodule

```

information of the target. This process is usually realized by TDC. In order to suppress the interference of ambient light, an effective way is to shoot the laser multiple times and collect the data for histogram statistics to obtain peak information. This circuit can be implemented on-chip or off-chip. The advantage of on-chip implementation is that it can directly output the processed data and reduce the data rate, but this will take up a lot of chip area for storing and computing [14].

When performing histogram processing, different bin values determine the reliability and accuracy of the obtained peak position, that is, the TOF value. The larger the bin value, the more photons collected in a single bin, and the higher reliability of the peak information, but a too large bin value will introduce a lot of quantization noise, which will restrict the accuracy of the measurement. Therefore, the bin value should be carefully selected, and usually it is consistent with the LSB of the TDC.

For behavior-level modeling of the histogram module, we can set an periodic signal BIN, whose half period is consistent with the bin value as input, which accumulates the number of incident photons (The number of rising edges of the input signal SIGNAL) in the interval corresponding to consecutive rising edges and stores them in the variable NUM, then pass the value of NUM to the output signal OUT and reset it at the end, and repeat this process until the histogram results for the entire interval are obtained. The pseudocode is as follows.

Taking the histogram processing in first-hit mode as an example, the used key model parameters are as Table I. The theoretical value of the target distance as 15 m, and the lasershot number of N as follows: $N = 1$, $N = 10$, $N = 100$. Then the output histogram result in first-hit mode is shown in Fig. 10.

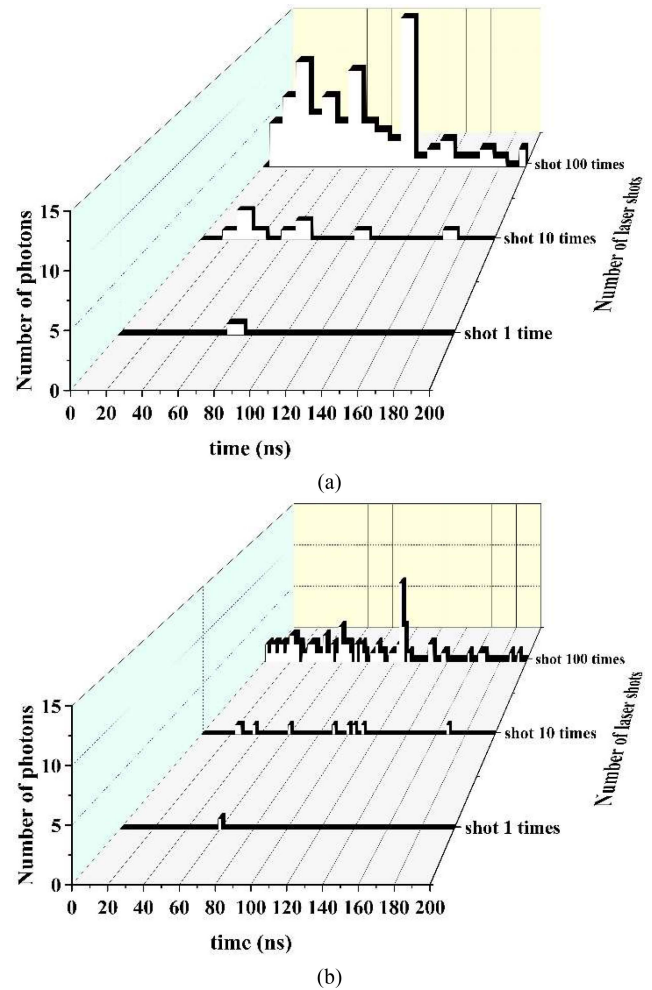


Fig. 9. Output histogram results of the behavioral model in first-hit mode (a) bin value = 10 ns; (b) bin value = 2 ns.

It can be seen from Fig. 9 that the result obtained by single laser shot is unreliable due to the interference of ambient light. As the number of shot times increases, the test results are closer to the real value. At the same time, it can be seen from the results of 100 times in Fig. 9(a) that before the arrival of signal photons, many erroneous results will be recorded due to false triggering of ambient light. When the ambient light power increases further, even if the signal light power is high, it is difficult to get the correct result, which is the so-called pile-up effect. This is consistent with our conclusion in Section III. Similarly, we can also use this model for multi-event mode to further compare the differences between the two modes. It can be seen from Fig. 10 that for the same ambient photons and signal photons rate, the peak value obtained by using the multi-event mode is significantly higher than that obtained by the first-hit mode, which increases by nearly 4 times. This further verifies the conclusion we got in Section III that multi-event mode can effectively suppress the pile-up effect. We selected multiple sets of results with different ambient light intensity, target distance, and bin width for comparison, and the number of laser shooting is 100.

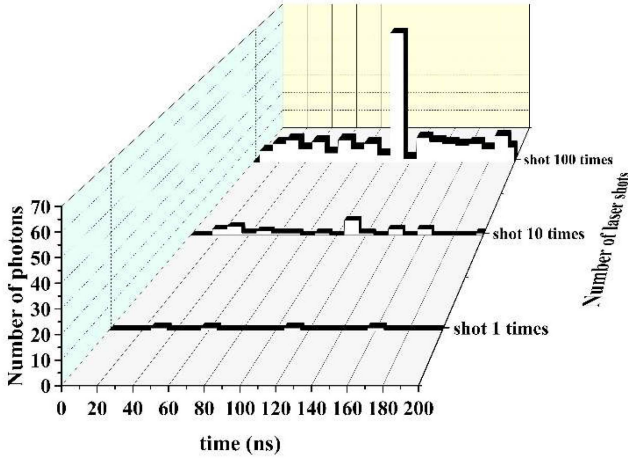


Fig. 10. Output histogram results of the behavioral model in multi-event mode with bin value = 10 ns.

TABLE II
HISTOGRAM MODELING RESULTS FOR MULTIPLE EVENT PATTERNS

target distance	ambient light intensity	bin width	Simulation distance	$\frac{PEAK_s}{PEAK_n}$
10m	20klux	2ns	9.90m	6.0
10m	20klux	5ns	9.75m	6.4
10m	50klux	5ns	9.75m	3.1
20m	20klux	2ns	20.1m	2.0
20m	20klux	5ns	19.5m	3.0
20m	50klux	5ns	19.5m	1.5

As shown in Table II, When a larger bin value (5 ns bin width) is used, the value of $PEAK_s/PEAK_n$ is very high, which means that this mode has a high ability to resist noise interference. But the accuracy is limited within 5 ns. When a smaller bin value (2 ns bin width) is used, although the value of $PEAK_s/PEAK_n$ decrease, the accuracy of the results can be further improved. Of course, if the selected bin value is too small, it may lead to incorrect measurement results, and even high accuracy is meaningless. The above results indicate that the behavior level model can accurately predict the results under multiple event modes, which has important significance for the determination of relevant parameters.

Another way to suppress ambient light interference is to use coincident detection circuits. The basic principle is to construct macro pixels by combining SPAD output signals into one signal, and then set a time window (generally equal to the laser pulse width), in which each pixel is turned on at the same time, and the incoming photons are continuously monitored. For the case where the set threshold is reached, it is considered as a signal photon and stored, otherwise it is an ambient photon, so as to achieve the purpose of screening photons [15], [16].

In [9], the coincident detection is mathematically modeled, and the function of the coincident detection module is described as “photon rate” to “event rate”, and the lower the photon rate, the stronger the suppression effect, and the higher the photon rate, the weaker the suppression effect. The parameters that need to be

Algorithm 2: Verilog-A HDL Pseudocodes for CD Module.

```

module CD(PHOTON, OUT);
  input PHOTON; // Photons
  parameter real TWIN; //time window width
  parameter real TH; // threshold
  voltage OUT, PHOTON;
  real PULSE, NUM, OUTEND;
  real T0; //timestamp
  /*****define function*****/
  analog begin
    @(initial_step) begin
      PULSE = 0;
      NUM = 0;
      T0 = 0;
      OUTEND = 0;
    end
    @(cross(V(PHOTON) - TH, +1))
      if(PULSE < 1) begin
        T0 = $abstime;
        PULSE = 1;
      end
      else PULSE = PULSE;
    @(timer(T0 + TWIN)) PULSE = 0;
    @(cross(V(PHOTON) - TH, +1)) begin
      NUM = NUM + 1;
      if(NUM >= TH_CD)
        OUTEND = 1;
      else OUTEND = 0;
    end
    @(cross(PULSE - TH, -1)) begin
      OUT_END = 0;
      NUM = 0;
    end
    V(OUT)<+transition(OUTEND * 1.8, td, tt);
  end
endmodule

```

considered in modeling the coincident detection circuit include the number of pixels in the macropixel, the detection window, and the detection threshold.

For behavior-level modeling of the CD module, an initial low-level signal PULSE can be used as a response to the input PHOTON. When the first photon arrives, the PULSE jumps to a high level and records the moment T0. After TWIN, reset the PULSE to Low level, during this period, the rising edge of PHOTON is processed through the NUM signal. When the threshold value TH_CD is just reached, the output OUT_END jumps to a high level, and then the above process is repeated to achieve the output after concurrent detection.

Using the same data of first-hit mode in Table I, and setting the bin value as 10 ns. The parameters related to coincident detection are shown in Table III. The obtained coincident detection results are shown in Fig. 11.

Comparing the histogram results in Figs. 9(a) and 11, it is not difficult to find that the accumulated histogram data of ambient

TABLE III
PARAMETERS USED IN COINCIDENT DETECTION

Parameter	Description	Value
N	the number of pixels	4
TWIN	detection window	5ns
TH_CD	detection threshold	2

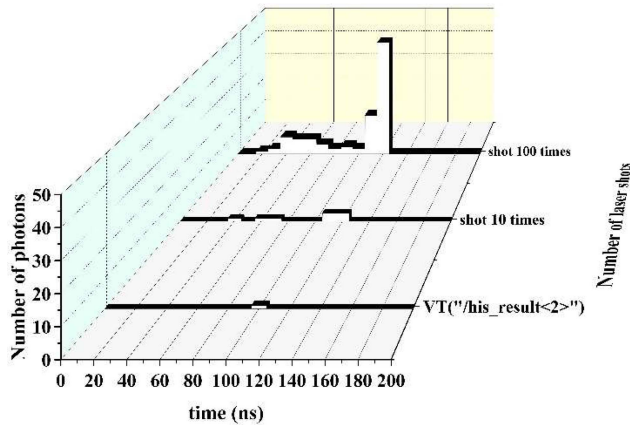


Fig. 11. Output histogram results of coincident detection circuit modeling.

light before the arrival of signal light is significantly reduced. The SBR_{hist} for coincident detection is 5, and the $SBR_{hist,cd}$ for coincident detection can be increased to 13, corresponding an improvement of nearly 2.6 times. This is consistent with the conclusion in [9].

VI. CONCLUSION

This paper theoretically analyzes the multi-event mode and time-gating method in the SPAD-based image sensor, and compares the change of detection probability before and after the implementation of these methods. A comprehensive behavior-level model is proposed in this paper, which can quickly and accurately analyze the above theoretical analysis and various noise reduction methods, thereby significantly improving design efficiency. The simulation results of the proposed behavioral modeling are consistent with the theoretical analysis, which shows it can be used to accurately predict the effect of the adopted noise reduction method and the function of each circuit module in the LiDAR system.

REFERENCES

- [1] R. Horaud et al., "An overview of depth cameras and range scanners based on time-of-flight technologies," *Mach. Vis. Appl.*, vol. 27, no. 7, pp. 1005–1020, 2016.
- [2] T. Talala, E. Parkkinen, and I. Nissinen, "CMOS SPAD line sensor with fine-tunable parallel connected time-to-digital converters for raman spectroscopy," *IEEE J. Solid-State Circuits*, vol. 58, no. 5, pp. 1350–1361, May 2023, doi: [10.1109/JSSC.2022.3212549](https://doi.org/10.1109/JSSC.2022.3212549).
- [3] S. Moazeni, K. Renehan, E. H. Pollmann, and K. L. Shepard, "An integrated-circuit node for high-spatiotemporal resolution time-domain near-infrared diffuse optical tomography imaging arrays," *IEEE J. Solid-State Circuits*, vol. 58, no. 5, pp. 1376–1385, May 2023, doi: [10.1109/JSSC.2022.3223854](https://doi.org/10.1109/JSSC.2022.3223854).
- [4] J. Kostamoavaara, S. Jahromi, L. Hallman, G. Duan, J.-P. Jansson, and P. Keränen, "Solid-state pulsed time-of-flight 3-D range imaging using CMOS SPAD focal plane array receiver and block-based illumination techniques," *IEEE Photon. J.*, vol. 14, no. 2, Apr. 2022, Art. no. 6817911, doi: [10.1109/JPHOT.2022.3153487](https://doi.org/10.1109/JPHOT.2022.3153487).
- [5] P. Padmanabhan, C. Zhang, and E. Charbon, "Modeling and analysis of a direct time-of-flight sensor architecture for LiDAR applications," *Sensors*, vol. 19, 2019, Art. no. 5464.
- [6] A. Tontini, L. Gasparini, and M. Perenzoni, "Numerical model of SPAD-based direct time-of-flight flash LiDAR CMOS image sensors," *Sensors*, vol. 20, 2020, Art. no. 5203.
- [7] D. Li, J. Hu, R. Ma, X. Wang, Y. Liu, and Z. Zhu, "SPAD-based LiDAR with real-time accuracy calibration and laser power regulation," *IEEE Trans. Circuits Syst. II: Exp. Briefs*, vol. 70, no. 2, pp. 431–435, Feb. 2023, doi: [10.1109/TCSII.2022.3211868](https://doi.org/10.1109/TCSII.2022.3211868).
- [8] M. Beer, J. F. Haase, J. Ruskowski, and R. Kokozinski, "Background light rejection in SPAD-based LiDAR sensors by adaptive photon coincidence detection," *Sensors*, vol. 18, 2018, Art. no. 4338.
- [9] M. Beer, O. M. Schrey, B. J. Hosticka, and R. Kokozinski, "Coincidence in SPAD-based time-of-flight sensors," in *Proc. 13th Conf. Ph.D. Res. Microelectronics Electron.*, 2017, pp. 381–384, doi: [10.1109/PRIME.2017.7974187](https://doi.org/10.1109/PRIME.2017.7974187).
- [10] Y. Xu, Z. Wu, and D. Li, "Behavioral modeling of photon arrival time for time-of-flight measurement circuit simulation," *IEEE Photon. J.*, vol. 11, no. 1, Feb. 2019, Art. no. 6800509, doi: [10.1109/JPHOT.2019.2893351](https://doi.org/10.1109/JPHOT.2019.2893351).
- [11] G. Chen, C. Wiede, and R. Kokozinski, "Data processing approaches on SPAD-based D-TOF LiDAR systems: A review," *IEEE Sensors J.*, vol. 21, no. 5, pp. 5656–5667, Mar. 2021, doi: [10.1109/JSEN.2020.3038487](https://doi.org/10.1109/JSEN.2020.3038487).
- [12] D. Bronzi, F. Villa, S. Tisa, A. Tosi, and F. Zappa, "SPAD figures of merit for photon-counting, photon-timing, and imaging applications: A review," *IEEE Sensors J.*, vol. 16, no. 1, pp. 3–12, Jan. 2016, doi: [10.1109/JSEN.2015.2483565](https://doi.org/10.1109/JSEN.2015.2483565).
- [13] F. Zappa, S. Tisa, A. Tosi, and S. Cova, "Principles and features of single-photon avalanche diode arrays," *Sens. Actuators A, Phys.*, vol. 140, no. 1, pp. 103–112, Oct. 2007.
- [14] I. Gyongy, N. A. W. Dutton, and R. K. Henderson, "Direct time-of-flight single-photon imaging," *IEEE Trans. Electron Devices*, vol. 69, no. 6, pp. 2794–2805, Jun. 2022, doi: [10.1109/TEDE.2021.3131430](https://doi.org/10.1109/TEDE.2021.3131430).
- [15] C. Niclass, M. Soga, H. Matsubara, S. Kato, and M. Kagami, "A 100-m range 10-frame/s 340 x 96-pixel time-of-flight depth sensor in 0.18um CMOS," *IEEE J. Solid-State Circuits*, vol. 48, no. 2, pp. 559–572, Feb. 2013.
- [16] C. Niclass, M. Soga, H. Matsubara, M. Ogawa, and M. Kagami, "A 0.18um CMOS SoC for a 100-m-range 10-frame/s 200 x 96-pixel time-of-flight depth sensor," *IEEE J. Solid-State Circuits*, vol. 49, no. 1, pp. 315–330, Jan. 2014, doi: [10.1109/JSSC.2013.2284352](https://doi.org/10.1109/JSSC.2013.2284352).